state is higher. Therefore balance gradients in the ablation zone tend to become larger. With regard to δB_m, the effect is greatest on glaciers in a wet climate. Finally, the albedo feedback contributes more to the sensitivity when precipitation rates are higher.

Results for the summer warming of +1 K (June, July, and August) show a cut-off in the increase of sensitivity in glaciers in moist climates. The occurrence of a cut-off is understandable because the melting on moist glaciers takes place not only in summer but also in fall and spring. Therefore the duration of the melt season will not increase when summer temperature goes up.

Further calculations were based on the assumption that each coherent glacierized region may be characterized by two quantities: the annual precipitation P_k and the glacier area A_k (Fig. 4). The subscript k now refers to the particular region. To arrive at a reliable estimate of the global mean sensitivity, we divided all glaciers into 100 regional groups (8) and assigned to each group a characteristic value of the annual precipitation, based on climatological maps and data from climatological stations. This is not a trivial matter, as glaciers and ice caps tend to form in the wettest parts of terrain with a pronounced topography. Precipitation rates taken from maps and weather stations will therefore underestimate P. On the basis of a comparison between the precipitation rates obtained from maps and from the mass-balance studies on the 12 selected glaciers, we used:

$$P_k = \max\{1.25P_{map};\ 0.22\}$$

where P_k is given in meters per year.

The area-weighted mean change in B_m for a uniform 1-K warming is −0.395 m/yr. As the ratio of glacier area to ocean area is 0.00146, this value corresponds to a sea-level rise of 0.577 mm/yr. In comparison, Meier's calculation showed that from 1900 to 1961 glaciers contributed 28 mm (best estimate) to sea-level rise (*3*). A linear fit of Jones' (*9*) temperature data for this period yields a global annual mean temperature rise of 0.29 K. The same procedure applied to Hansen and Lebedeff's (*10*) data gives a rise of 0.41 K. For the purpose of estimating a sensitivity we assume that the temperature rise has been 0.35 K. Meier's estimate of 28 mm of sea-level rise in 60 years would then convert to a rate of 1.33 mm/yr for a 1 K warming. This value is twice that obtained by our modeling approach. However, the error assigned to Meier's estimate was 0.73 mm/yr, so our value is just at the lower bound of his estimate.

The discrepancy can to a large extent be explained by the large spatial variability of temperature trends, which make the empirical estimate of glacier sensitivity given above invalid. Also, in earlier estimates of glacier sensitivity, the subpolar ice caps, which have such a low sensitivity, were assigned too small of a weight. Here we only modeled two subpolar ice caps, both located in Canada. In future studies other small ice caps in the Arctic should be considered.

It has been argued that glacier melt resulting from increasing temperatures could be offset by higher precipitation. We investigated this notion by increasing the precipitation rate in the model by 10% in the case of a 1 K warming. Such a change would be large indeed, at least on the global scale. The result is a reduction of the rate of sea-level rise to 0.329 mm/yr. It thus appears that even a significant increase in precipitation cannot compensate for increased melting, and further shrinkage of glaciers and small ice caps must occur in a warmer climate.

REFERENCES AND NOTES

1. W. Haeberli *et al.*, *World Glacier Inventory: Status 1988* (International Association of Hydrological Sciences, Paris, 1989).
2. R. A. Warrick and J. Oerlemans, in *Climate Change—The IPCC Scientific Assessment* (World Meteorologic Organization–United Nations Environment Programme, Cambridge Univ. Press, New York, 1990), pp. 257–281.
3. M. F. Meier, *Science* **226**, 1418 (1984).
4. The annual balance amplitude is defined as $(b_w - b_s)/2$, where b_w is the winter balance (positive) and b_s the summer balance (negative). These quantities are normally measured in field programs on glaciers.
5. International Association of Scientific Hydrology, *Fluctuations of Glaciers* (Unesco, Paris, 1967, 1973, 1977, 1985, and 1988), vols. 1 to 5.
6. J. Oerlemans and N. C. Hoogendoorn, *J. Glaciol.* **35**, 399 (1989).
7. J. Oerlemans, *J. Glaciol.*, in press.
8. Data were taken from many sources, notably (*1*).
9. P. D. Jones, *Clim. Monit.* **18**, 80 (1989).
10. J. Hansen and S. Lebedeff, *J. Geophys. Res.* **92**, 13345 (1987).
11. This research was sponsored by the Dutch National Research Programme on Global Air Pollution and Climate Change (contract 276/91-NOP) and by the Commission of the European Communities (contract EPOC-CT90-0015).

26 May 1992; accepted 28 July 1992

Sulfate Cooling Effect on Climate Through In-Cloud Oxidation of Anthropogenic SO_2

Jos Lelieveld and Jost Heintzenberg

Anthropogenic SO_2 emissions may exert a significant cooling effect on climate in the Northern Hemisphere through backscattering of solar radiation by sulfate particles. Earlier estimates of the sulfate climate forcing were based on a limited number of sulfate-scattering correlation measurements from which a high sulfate-scattering efficiency was derived. Model results suggest that cloud processing of air is the underlying mechanism. Aqueous phase oxidation of SO_2 into sulfate and the subsequent release of the dry aerosol by cloud evaporation render sulfate a much more efficient scatterer than through gas-phase SO_2 oxidation.

Sulfur dioxide (SO_2) emissions from fossil fuel combustion may have a climate cooling effect through the backscattering of solar radiation by sulfate particles in cloud-free regions (*1, 2*). Sulfate aerosol forms in the atmosphere by oxidation of SO_2 either in the gas phase followed by condensation of the sulfuric acid produced or in the aqueous phase of clouds that subsequently evaporate (*3*). In the atmosphere SO_2 and sulfate have a combined lifetime of about 1 to 1.5 weeks, during which they can be transported several thousands of kilometers (*4*). Because vertical exchange between the lower and upper troposphere is relatively slow, the sulfate forcing on climate is exerted predominantly in the lower troposphere of the Northern Hemisphere, where anthropogenic SO_2 emissions are strongest. The mean negative climate forcing by sulfate in the Northern Hemisphere has been estimated at about $-1.1\ \mathrm{W\ m^{-2}}$ (*1*), comparable to the positive forcings of about 1.5 and 0.95 $\mathrm{W\ m^{-2}}$ caused by increases of CO_2 concentrations and of other greenhouse gases, respectively (*5*). Sulfate climate forcing in the Southern Hemisphere may be about $-0.1\ \mathrm{W\ m^{-2}}$ (*1*). In this report we show that in-cloud SO_2 oxidation followed by cloud evaporation, which results in the addition of sulfate only to that subset of particles that has served as cloud condensation nuclei, strongly influences the scattering properties of the aerosol.

The above estimates of sulfate climate forcing are critically dependent on the optical thickness δ of the aerosol layer, described in Lambert's law of radiation extinction

$$E_\lambda = E_{0,\lambda} e^{-\delta} \qquad (1)$$

$E_{0,\lambda}$ is the solar irradiance incident to the aerosol layer ($\mathrm{W\ m^{-2}}$), E_λ is the irradiance reaching the Earth's surface. Aerosol ex-

---

J. Lelieveld, Max-Planck Institute for Chemistry, Atmospheric Chemistry Division, Post Office Box 3060, D-6500 Mainz, Germany.
J. Heintzenberg, Department of Meteorology, University of Stockholm, S-10691 Stockholm, Sweden.

tinction is the combined effect of absorption and scattering; both remove energy from the incident beam. Because sulfate does not absorb solar radiation, extinction equals scattering. The optical thickness of sulfate aerosol can be determined by the product of the mass-scattering coefficient of sulfate α ($m^2\ g^{-1}$) and the sulfate burden $B_{SO_4^{2-}}$ ($g\ m^{-2}$)

$$\delta = \alpha\, B_{SO_4^{2-}} \qquad (2)$$

On the basis of aircraft measurements over southern Sweden (6), Charlson *et al.* (*1*) adopted an empirical value of $\alpha = 8.5\ m^2\ g^{-1}$. This mass-scattering coefficient, derived from a correlation between sulfate amount and light-scattering, implies that sulfate is very efficient in scattering solar radiation. In these measurements, however, 40 to 60% of the light-scattering material measured was not sulfate. Hence, a causal relation between aerosol chemical composition and scattering properties was not demonstrated.

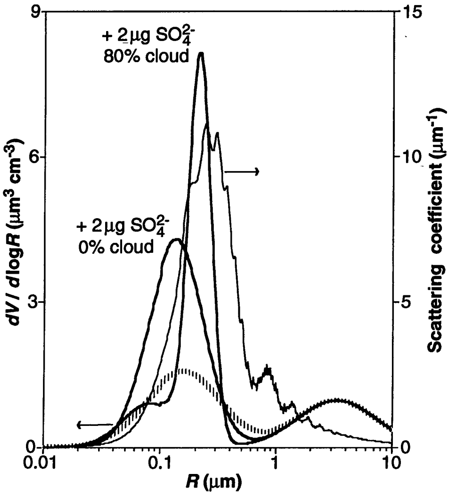

Fig. 1. Measured clean continental aerosol volume size distribution [dashed curve; adopted from (*19*)] and anthropogenically perturbed volume size distributions (thick solid lines). The latter have been calculated by addition of 2 µg m^{-3} sulfate to the clean continental aerosol through the gas phase alone, and through cloud processing, for the assumption that 80% of the sulfate is formed by SO_2 oxidation in the aqueous-phase. The volume size distribution of the cloud processed aerosol is narrower but has a higher maximum because the cloud processing causes preferential deposition of sulfate on a subset of the aerosol. The thin solid line shows the volume-normalized scattering coefficient ($\sigma^V_{s,\lambda}$) at λ = 0.55 µm.

The particle-scattering efficiency factor, $Q_{s,\lambda}$, a relative measure of the light attenuation ability of the aerosol, varies between 0 and about 5, depending on the wavelength λ, particle size, and particle composition (7). A value of $Q_{s,\lambda}$ of 2 means that the particle removes twice the amount of parallel light beams as its projected disk, which is the result of direct light interception, refraction, and diffraction (8). The scattering cross section of a particle (assumed spherical) is the product of $Q_{s,\lambda}$ and its geometric cross section πR^2, where R is the particle radius. A volume-normalized scattering coefficient, $\sigma^V_{s,\lambda}$ (m^{-1}), is

$$\sigma^V_{s,\lambda} = Q_{s,\lambda}\frac{\pi R^2}{4/3\pi R^3} \qquad (3)$$

which we use later (Fig. 1) to illustrate how the particle size distribution is affected by sulfur chemistry, and in turn controls the aerosol-scattering properties. The scattering coefficient of a population of particles, $\sigma_{s,\lambda}$ (m^{-1}), is determined by the integral of the scattering cross section over the particle radii and the number concentration, $N(R)$ (m^{-3})

$$\sigma_{s,\lambda} = \int_0^\infty Q_{s,\lambda}\pi R^2 N(R)dR \qquad (4)$$

If the aerosol particles are small compared to the wavelength, defined as the Rayleigh regime ($R << 0.55$ µm for visible radiation), scattering computations are relatively simple. For example, for a sulfate particle with $R = 0.05$ µm, $Q_{s,\lambda} \approx 0.02$, and the backscattered fraction of light, β, is 0.5 ($\lambda = 0.55$ µm). For larger particles Mie theory must be applied, although for $R >> 0.55$ µm, for example, for cloud and rain droplets, $Q_{s,\lambda}$ converges to a value of about 2 (7). Calculations for the intermediate aerosol size range, the Mie regime, are extensive because of the complicated interactions of electromagnetic radiation with bodies having dimensions comparable to the wavelength. Particles that grow from the Rayleigh into the Mie regime, for instance, hygroscopic nuclei that deliquesce in a humid environment, become much more efficient light scatterers than particles in the Rayleigh regime. However, the backscattered fraction also decreases, typically to $\beta \approx 0.1$. As a consequence of the oscillatory and highly complex behavior of atmospheric scatterers in the Mie regime, it is difficult to predict offhand the radiative effect of an increase in sulfate. Therefore, we applied an algorithm based on the formal Mie theory of the interactions of solar radiation with dielectric spheres (9) to simulate changes in aerosol-scattering properties caused by anthropogenic sulfur emissions.

Using more than 10 years of worldwide observations of cloud coverage, compiled in cloud atlases (*10*), Lelieveld *et al.* (*11, 12*) derived the mean volume fraction of air that is occupied by clouds as function of season, latitude, and altitude. On a global average, the volume fraction of clouds in the troposphere was inferred to be about 5 to 6% (excluding cirrus). Further derivations yielded the average time that air spends inside clouds per passage (~3 hours) and outside clouds; taken together, the mean cloud cycle time is about 1 to 2.5 days. Because the mean sulfate lifetime is about 1 week (*13*), it follows that the sulfate goes through about 3 to 7 cloud condensation-evaporation events before being removed from the atmosphere. Moreover, as sulfate is efficiently removed by rain but inefficiently by dry deposition (*14*), this

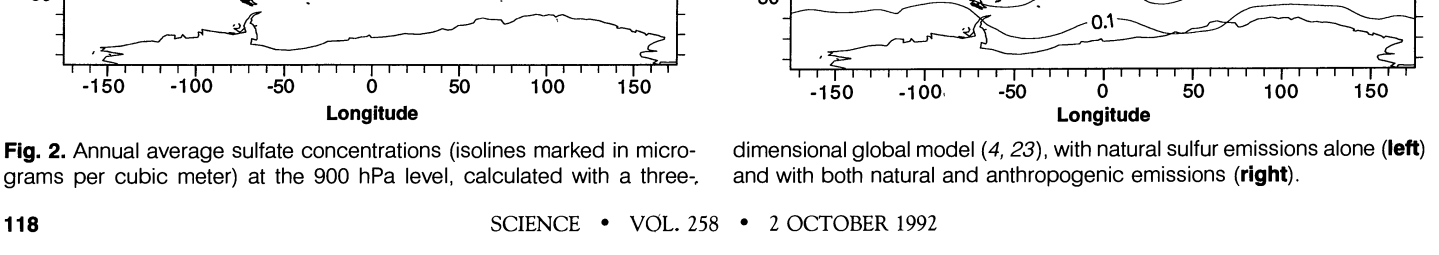

Fig. 2. Annual average sulfate concentrations (isolines marked in micrograms per cubic meter) at the 900 hPa level, calculated with a three-dimensional global model (*4, 23*), with natural sulfur emissions alone (**left**) and with both natural and anthropogenic emissions (**right**).

Table 1. Calculated sulfate aerosol-scattering properties; $\sigma_{s,\lambda}$ is the particle-scattering coefficient, α is the sulfate mass-scattering coefficient, and β is the hemispheric backscattered fraction (all for λ = 0.55 μm).

Aerosol ΔSO_4^{2-} ($\mu g\ m^{-3}$)	Clouds	$\sigma_{s,\lambda}$ (μm^{-1})	α ($m^2 g^{-1}$)	β
		*Unperturbed**		
—	—	7.7	—	0.11
		Perturbed		
0.5	No	8.6	1.8	0.13
0.5	Yes	11.6	7.8	0.09
1	No	10.5	2.8	0.12
1	Yes	14.7	7.1	0.09
2	No	14.7	3.5	0.12
2	Yes	20.8	6.6	0.09
5	No	28.9	4.2	0.11
5	Yes	38.5	6.2	0.09
10	No	54.7	4.7	0.10
10	Yes	65.9	5.8	0.09

*A continental aerosol measured at the remote site Goldstone (California) under clean conditions (*19*).

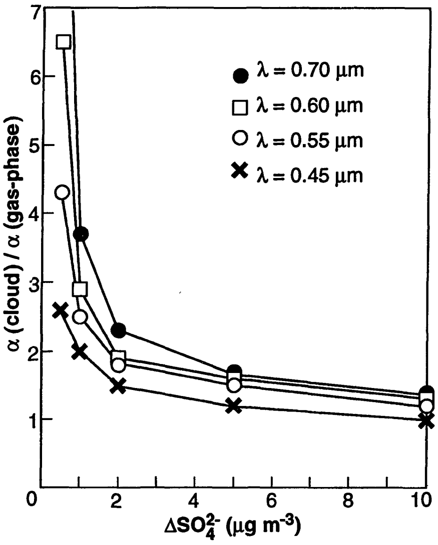

Fig. 3. Sulfate perturbation (ΔSO_4^{2-}) and wavelength (λ) dependence of the aerosol mass-scattering coefficient as calculated after cloud processing, α(cloud), relative to that of the aerosol influenced by gas phase deposition of sulfate alone, α(gas phase). It follows that cloud processing enhances scattering relatively more at longer wavelengths and relatively less at large sulfate perturbations.

calculation also confirms that most clouds evaporate rather than precipitate (*15*). On the basis of these and similar estimates, combined with transport-chemistry model simulations, it has been calculated that the SO_2 lifetime (τ_{SO_2}) due to aqueous-phase oxidation is limited to a few days only, whereas gas-phase conversion of SO_2 leads to a τ_{SO_2} of weeks to months, depending on latitude and season. Hence, on average, 80 to 90% of the transformation of SO_2 to sulfate takes place in clouds (*4, 12, 16*). Consequently, deposition of newly formed sulfate on pre-existing particles occurs to a large extent on a subset of the aerosol, namely on those particles that were large enough to have acted as cloud condensation nuclei (CCN); the sulfate can be released again through cloud evaporation. The minimum CCN radius varies between about 0.05 and 0.2 μm, depending on the water vapor supersaturation (determined by the vertical air velocity) and the total number of hygroscopic particles competing for the moisture (*15, 17, 18*).

The aerosol model we developed, which has been coupled to the Mie routine mentioned earlier, simulates deposition of prescribed amounts of sulfate on a remote continental aerosol, as measured by Whitby and Sverdrup (*19*) (see Fig. 1). This aerosol reflects clean conditions, although traces of anthropogenic origin cannot be ruled out. In the model simulations, sulfate deposition on the aerosol in cloud-free conditions is proportional to the particle surface area. In addition, the aerosol mass was increased by about 10% of the sulfate added, because of deliquescence at 70 to 80% relative humidity, as suggested by measurements of a continental background aerosol (*20*). The formation of new particles was neglected because this takes place under rather special conditions, such as high relative humidity and low pre-existing particle number concentration (*21*). Moreover, it can be expected that the fate of newly formed small particles in continental aerosol is dominated by coagulation with pre-existing particles. For simulation of cloudy conditions (cloud processing of air) we assumed that 80% of the sulfate was produced in the aqueous phase, that the CCN minimum radius R_{min} was 0.1 μm, and that 80% of the CCN became activated to form cloud droplets (*17, 22*). Furthermore, cloud droplets were assumed to be monodisperse; every droplet received an equal amount of sulfate. The calculated size distributions of the aerosols that resulted from cloud evaporation and the distributions affected by the sulfate added through the gas phase alone were used to perform the Mie scattering computations. The sulfate increases due to anthropogenic SO_2 emissions were calculated with a three-dimensional global transport chemistry model (*23*). Simulations with natural emissions of dimethyl sulfide and SO_2 equaling 31 Tg S per year were compared with simulations in which anthropogenic SO_2 emissions of 73.5 Tg S per year were also included (*4*) (Fig. 2). We performed five aerosol perturbation experiments, assuming anthropogenic sulfate increases (ΔSO_4^{2-}) of 0.5, 1, 2, 5, and 10 μg m^{-3}. These values are considered to be representative of a range of pollution conditions, from local to continental scales.

As shown in Fig. 1, the particle size distribution (on a volume basis) of the cloud-processed aerosol is narrower, but has a maximum at larger radius compared to the size distribution of the aerosol influenced by gas-phase deposition alone. A characteristic local minimum occurred at $R \approx 0.1$ μm in the cloud-processed aerosol; this results from the preferential deposition of sulfate on particles that have previously served as CCN, hence on particles with $R > 0.1$ μm. Shipborne measurements in the marine boundary layer, where aerosol size distributions are dominated by sulfate particles (*24*) and where clouds recur commonly, confirm that these size distributions are real (*25*). The double-peaked shape (at $R \approx 0.1$ μm) of aerosol size distributions in more polluted continental air may be obscured by gas-phase deposition of gases and small particles other than sulfate on the aerosol; sulfate usually contributes considerably less than half of the aerosol mass (*13, 14*).

The results (Table 1) show clearly that the cloud-processed aerosol is much more efficient at scattering than the aerosol that has received the sulfate only through the gas phase. The reason is that through clouds the sulfate is preferentially added to the particles in the size range associated with the maximum of the scattering curve in Fig. 1. On the other hand, the backscattered fraction β also changes; it decreases from about 0.11 to 0.09 for the cloud processed aerosol, whereas in contrast β can actually increase for the aerosol affected by the gas-phase alone (Table 1). To quantify this in terms of climate forcing, we compare our results with those of Charlson *et al.* (*1*), who adopted a mean backscattered fraction of $\beta = 0.15$. We derive the sulfate mass-scattering coefficient α by

$$\alpha = \frac{\Delta\sigma_{s,\lambda}}{\Delta SO_4^{2-}} \qquad (5)$$

in which $\Delta\sigma_{s,\lambda}$ is the difference between the scattering coefficients for the pristine and the perturbed aerosols (Table 1). The calculated values for α when only gas-phase deposition is considered are considerably lower than the empirical value of $\alpha = 8.5$ $m^2\ g^{-1}$ adopted by Charlson *et al.* (*1*). Applying the α values for the aerosol in which sulfate is produced only through the gas phase ($1.8\ m^2\ g^{-1} \le \alpha$(gas phase) ≤ 4.7 $m^2\ g^{-1}$) to the sulfate perturbations indicated in Fig. 2 would result in a sulfate climate forcing in the Northern Hemisphere of about -0.3 W m^{-2}. However, cloud processing yields $5.8\ m^2\ g^{-1} \le \alpha$(cloud) ≤ 7.8 $m^2\ g^{-1}$, depending on the sulfate perturbation exerted (Table 1). The differences between the α values of cloud-processed sulfate and those of sulfate added only by gas-phase conversion decrease with increasing ΔSO_4^{2-}. Cloud processing is relatively less efficient in enhancing scattering for large ΔSO_4^{2-}, in part because for perturbations through gas-phase conversion only, α increases with ΔSO_4^{2-} (Table 1). In fact, the ratio α(cloud)/α(gas phase) approximates unity for large values of ΔSO_4^{2-} (Fig. 3). Nevertheless, considering the calculated average sulfate pollution of about 0.5 to $2\ \mu g\ m^{-3}$ in the lower atmosphere in a large part of the Northern Hemisphere (Fig. 2), we conclude that the mean climate forcing by sulfate in this part of the globe may be about -0.5 to $-1.0\ W\ m^{-2}$, to a large extent caused by in-cloud oxidation of anthropogenic SO_2.

REFERENCES AND NOTES

1. R. J. Charlson, J. Langner, H. Rodhe, *Nature* **348**, 22 (1990); R. J. Charlson, C. B. Leovy, S. G. Warren, *Tellus* **43AB**, 152 (1991).
2. T. M. L. Wigley, *Nature* **349**, 503 (1991).
3. J. G. Calvert *et al.*, *ibid.* **317**, 27 (1985).
4. J. Langner and H. Rodhe, *J. Atmos. Chem.* **13**, 225 (1991).
5. Intergovernmental Panel on Climate Change (IPCC), *Report of Working Group I* (Cambridge Univ. Press, Cambridge UK, 1990).
6. A. P. Waggoner *et al.*, *Nature* **261**, 120 (1976).
7. H. C. Van de Hulst, *Light Scattering by Small Particles* (Wiley, New York, 1957).
8. G. Mie, *Ann. Phys.* **25**, 377 (1908).
9. J. V. Dave, *IBM Sci. Cent. Rep. 320-3237* (IBM, Palo Alto CA, 1968).
10. S. G. Warren, C. J. Hahn, J. London, R. M. Chervin, R. Jenne, *NCAR Tech. Note TN-273+STR* (NCAR, Boulder CO, 1986); *ibid. TN-317+STR.*
11. J. Lelieveld, P. J. Crutzen, H. Rodhe, *GLOMAC Rep. UDC 551.510.4, CM-74* (International Meteorological Institute, Stockholm, 1989).
12. J. Lelieveld, in *C, N, P and S Biogeochemical Cycles*, R. Wollast, Ed. (Kluwer Academic, Dordrecht, 1992).
13. P. Warneck, *Chemistry of the Natural Atmosphere* (Academic Press, San Diego, 1988).
14. R. Jaenicke, in *Landolt-Börnstein*, vol. 4: *Meteorology* (Springer-Verlag, Berlin, 1988), pp. 391–457.
15. H. R. Pruppacher and J. D. Klett, *Microphysics of Clouds and Precipitation* (Reidel., Dordrecht, 1978).
16. D. A. Hegg, *J. Geophys. Res* **90**, 3773 (1985).
17. S. Twomey, *Atmospheric Aerosols* (Elsevier, Amsterdam, 1977).
18. M. B. Baker and R. J. Charlson, *Nature* **345**, 142 (1990).
19. K. T. Whitby and G. M. Sverdrup, in *The Character and Origins of Smog Aerosols*, G. M. Hidy *et al.*, Eds. (Wiley, New York, 1980), pp. 477–525.
20. G. Hänel and K. Bullrich, *Beitr. Phys. Atmos.* **51**, 129 (1978).
21. J. H. Seinfeld, *Atmospheric Chemistry and Physics of Air Pollution* (Wiley, New York, 1986).
22. J. Heintzenberg, J. A. Ogren, K. J. Noone, L. Gärdneus, *Atmos. Res.* **24**, 89 (1989).
23. P. H. Zimmermann, J. Feichter, H. K. Rath, P. J. Crutzen, W. Weiss, *Atmos. Environ.* **23**, 25 (1989).
24. A. Mészáros and K. Vissy, *J. Aerosol Sci.* **5**, 101 (1974).
25. W. A. Hoppel and G. M. Frick, *Atmos. Environ.* **24A**, 645 (1990); W. A. Hoppel and R. E. Larson, *Geophys. Res. Lett.* **13**, 125 (1986).
26. We thank R. J. Charlson, P. J. Crutzen, C. Harris, T. Peter, and H. Rodhe for comments.

23 April 1992; accepted 21 August 1992

Immuno-PCR: Very Sensitive Antigen Detection by Means of Specific Antibody-DNA Conjugates

Takeshi Sano, Cassandra L. Smith, Charles R. Cantor

An antigen detection system, termed immuno–polymerase chain reaction (immuno-PCR), was developed in which a specific DNA molecule is used as the marker. A streptavidin–protein A chimera that possesses tight and specific binding affinity both for biotin and immunoglobulin G was used to attach a biotinylated DNA specifically to antigen–monoclonal antibody complexes that had been immobilized on microtiter plate wells. Then, a segment of the attached DNA was amplified by PCR. Analysis of the PCR products by agarose gel electrophoresis after staining with ethidium bromide allowed as few as 580 antigen molecules (9.6×10^{-22} moles) to be readily and reproducibly detected. Direct comparison with enzyme-linked immunosorbent assay with the use of a chimera–alkaline phosphatase conjugate demonstrates that enhancement (approximately $\times 10^5$) in detection sensitivity was obtained with the use of immuno-PCR. Given the enormous amplification capability and specificity of PCR, this immuno-PCR technology has a sensitivity greater than any existing antigen detection system and, in principle, could be applied to the detection of single antigen molecules.

Antibody-based detection systems for specific antigens are a versatile and powerful tool for various molecular and cellular analyses and clinical diagnostics. The power of such systems originates from the considerable specificity of antibodies for their particular epitopes. A number of recent antibody technologies, including genetic engineering of antibody molecules (*1*) and the production of catalytic antibodies (*2*) and bispecific antibodies (*3*), are allowing a rapid expansion in the applications of antibodies. We were interested in further enhancing the sensitivity of antigen detection systems. This should facilitate the specific detection of rare antigens, which are present only in very small numbers, and thus could expand the application of antibodies to a wider variety of biological and nonbiological systems.

Polymerase chain reaction (PCR) technology (*4*) has become a powerful tool in molecular biology and genetic engineering (*5*). The efficacy of PCR is based on its ability to amplify a specific DNA segment flanked by a set of primers. The enormous amplification capability of PCR allows the production of large amounts of specific DNA products, which can be detected by various methods. The extremely high specificity of PCR for a target sequence defined by a set of primers should avoid the generation of false signals from other nucleic acid molecules present in samples. We reasoned that the capability of antigen detection systems could be considerably enhanced and potentially broadened by coupling to PCR. Following these ideas, we have developed an antigen detection system, termed immuno-PCR, in which a specific antibody-DNA conjugate is used to detect antigens.

In immuno-PCR, a linker molecule with bispecific binding affinity for DNA and antibodies is used to attach a DNA molecule (marker) specifically to an antigen-antibody complex, resulting in the formation of a specific antigen-antibody-DNA conjugate. The attached marker DNA can be amplified by PCR with the appropriate primers. The presence of specific PCR products demonstrates that marker DNA molecules are attached specifically to antigen-antibody complexes, which indicates the presence of antigen. A streptavidin–protein A chimera that we recently designed (*6*) was used as the linker. The chimera has two independent specific binding abilities; one is to biotin, derived from the streptavidin moiety, and the other is to the Fc portion of an immunoglobulin G (IgG) molecule, derived from the protein A moiety. This bifunctional specificity both for biotin and antibody allows the specific conjugation of any biotinylated DNA molecule to antigen-antibody complexes.

To test the feasibility of this concept, we immobilized various amounts of an antigen on the surface of microtiter plate wells and detected them by immuno-PCR. Bovine serum albumin (BSA) was used as the antigen because of the availability of pure protein and monoclonal antibodies against it. The detection procedure used (*7*) is similar to conventional enzyme-linked immunosorbent assay (ELISA). Instead of an enzyme-conjugated secondary antibody directed against the primary antibody, as in

---

Department of Molecular and Cell Biology, University of California at Berkeley, Berkeley, CA 94720, and Division of Structural Biology, Lawrence Berkeley Laboratory, Berkeley, CA 94720.